ELECTROCONVECTIVE INSTABILITY IN A FLUID LAYER

D. C. Jolly and J. R. Melcher

CSR-TR -69-2 February 4, 1969

CENTER FOR SPACE RESEARCH
MASSACHUSETTS INSTITUTE OF TECHNOLOGY

ELECTROCONVECTIVE INSTABILITY IN A FLUID LAYER

D. C. Jolly and J. R. Melcher

CSR-TR -69-2 February 4, 1969

ELECTROCONVECTIVE INSTABILITY IN A FLUID LAYER

by

D. C. Jolly and J.R. Melcher

Department of Electrical Engineering, Massachusetts Institute of Technology

Cambridge, Massachusetts

Steady flows of a fluid of slight electrical conductivity under the influence of an applied electric field intensity are often unstable. A study is described to illustrate with experiments and an analytical model the fundamental aspects of a wide range of instabilities that are characterized by the incipience of steady cellular convection as the electric Hartmann number $H_e = \varepsilon E/\sqrt{\mu\sigma}$ is on the order of unity (ε is the permittivity, E the imposed electric field intensity, μ the viscosity, and σ the electrical conductivity). A nonuniform electric field is used to induce an unstable configuration of surface charge and electric field intensity at a planar interface. The resulting instability leads to cellular convection in the plane of the interface. Predictions of the electric Hartmann number and wavelength for incipience of instability compare favorably to measurements. The dependence of the measured cellular convection velocity, resulting from the instability, on electric Hartmann number and electric Reynolds number are also in satisfactory agreement with the predictions from the simple model.

I. INTRODUCTION

A. Background

The history of fluid mechanics amply illustrates that the physical significance of a steady flow cannot be fully appreciated without examining its stability. There is considerable empirical evidence that electrohydrodynamic flows, for example in pumps and generators, or in image-processing devices involving electric fields and fluids, are even more likely to be unstable than ordinary steady flows. This is illustrated by the state of fine-scale turbulence often found as a fluid volume is stressed by electric fields, even in the absence of a mean flow. The relationship between laminar and turbulent electrohydrodynamic flows does not appear to be a simple extension of the physics of classic hydrodynamics.

There is an extensive literature of classes of electrohydrodynamic instability, largely at interfaces, that do not involve the electrical conduction process. By contrast, few problems of electrohydrodynamic instability where conduction is important have been brought to a rational state because they are often fraught with difficulties in reproducibility, and because the dependence on the particulars of the conduction process can render a given result of limited general value.

It is not our objective to give a review of electrohydrodynamic stability problems, but rather to use a particular physical situation as an illustration of the physical considerations which, through current findings, appear to be common to a wide class of instabilities. The steady flow configuration involves an electrical pumping of a liquid, in our case through the agent of electrical interfacial shear stresses.

An example of such pumping is Taylor's (1966) cellular convection interior and exterior to a liquid drop immersed in a second liquid stressed by an

electric field. Similar cellular convection induced by stresses from a nonuniform imposed field at a plane interface are investigated by Smith and Melcher (1967). A review relating largely to this class of flows and physical mechanisms for their instability serves as background for the following developments (Melcher & Taylor 1969), including studies of a similar instability (Malkus & Veronis 1961).

We wish to highlight three fundamental ingredients of electroconvective instabilities:

i. The configuration of charge density and electric field intensity required to give rise to the instability. This is the electrohydrodynamic analogue of the gravitational instability involving a layer of liquid supported by a less dense layer. This configuration is illustrated schematically in Fig. 1 for a one-dimensional dependence of the charge density q on the coordinate x. The configuration is potentially unstable if at some point

$$E_x Dq < 0 \qquad (1)$$

where E_x is the x component of the electric field intensity and $Dq \equiv dq/dx$. The instability condition of Eq. (1) is discussed by Turnbull and Melcher (1969) for the limit in which the effects of electrical conduction cannot be ignored. This leads to a second essential consideration.

ii. The role of charge relaxation in sustaining the unstable configuration of charge and field in the face of charge convection. In an Ohmic conductor, the free charge tends to relax with the time constant ε/σ, where ε is the permittivity and σ the electrical conductivity. Thus, effects of material convection in determining the

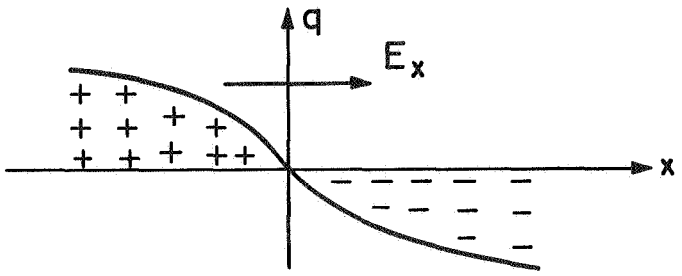

Fig. 1 Illustration of an unstable configuration of charge density q(x) and electric field intensity $E_x(x)$.

distribution of charge as given by Eq. (1) are in proportion to the ratio of a transport time U/b, (U and b respectively being the characteristic velocity and length), to the relaxation time. This ratio is the electric Reynolds number

$$R_e = \varepsilon U/\sigma b \tag{2}$$

Electroconvective instabilities are characterized by an appreciable effect of convection on the charge distribution; i.e., an appreciable R_e. However, the degree of charge convection required for instability is a matter of the competition between viscous and electrical stresses What constitutes "appreciable" convection depends on the third consideration;

iii. The ratio of the electrical stress acting on the convected charge to the viscous stress. In an Ohmic Newtonian fluid, an indication of this ratio is the electric Hartmann number

$$H_E = \varepsilon E/\sqrt{\mu\sigma} \tag{3}$$

where μ is the dynamic viscosity. Even though the effects of material convection on the charge distribution may be small (R_e is small compared to unity) the viscous retarding forces can be equally small. The electric Hartmann number thus indicates the conditions for incipient instability by comparing the electric stress acting on the convected charge to the viscous retarding stress.

It is the objective of the following sections to illustrate these three aspects of electroconvective instability with a case study that is easily produced and reproduced in experiments that give a clear visualization of the fluid motions. These objectives are met by developing a relatively simple model for the incipience of the instability and for the steady convection arising from

the instability. The model involves many judicious approximations made to avoid complexity which would obscure the basic mechanisms involved, but nevertheless retains the essential features of the interaction.

B. Phenomenon

First consider the steady flow. Figure 2a shows a cross-sectional view of a layer of slightly conducting liquid resting on strip electrodes alternately having the potentials V/2 and -V/2. Although only slightly conducting (typically corn oil), the liquid is nevertheless much more conducting than the air above. At least, according to an Ohmic conduction model, there is no space charge developed in the liquid bulk. However, charges are induced on the interface and, as sketched in Fig. 2a, these have the same sign as those on the nearest electrode. In consequence, there is an electrical surface force density acting in shear at the interface, as illustrated. In the section A-B of the interface, the electrical shear tends to pump the liquid toward the origin $x = 0$ just over the edges of the electrodes. The resulting cellular convection, with streamlines as shown, is the motion studied by Smith and Melcher (1967), and if "wrapped around on itself", is similar to Taylor's cellular convection within a drop (1966).

Our point here is that the configuration of charge and field at the interface is potentially unstable, and in fact characterizes electrohydrodynamic pumping configurations not only at interfaces, but also in the bulk of liquids. The configuration of surface charge and electric field intensity at the interface is essentially that of Fig. 1. The cellular motion in the x-z plane is often difficult to observe; rather, cells are observed to form in the x-y plane of the interface, as sketched in Fig. 2b. Note that with the fluid stationary, there are no surface stresses in the y direction, such as

Fig. 2a) A layer of slightly conducting liquid bounded from above by air and from below by strip electrodes at alternate polarities. Electrical shear stresses at the interface tend to pump the fluid in the cellular flow pattern shown.

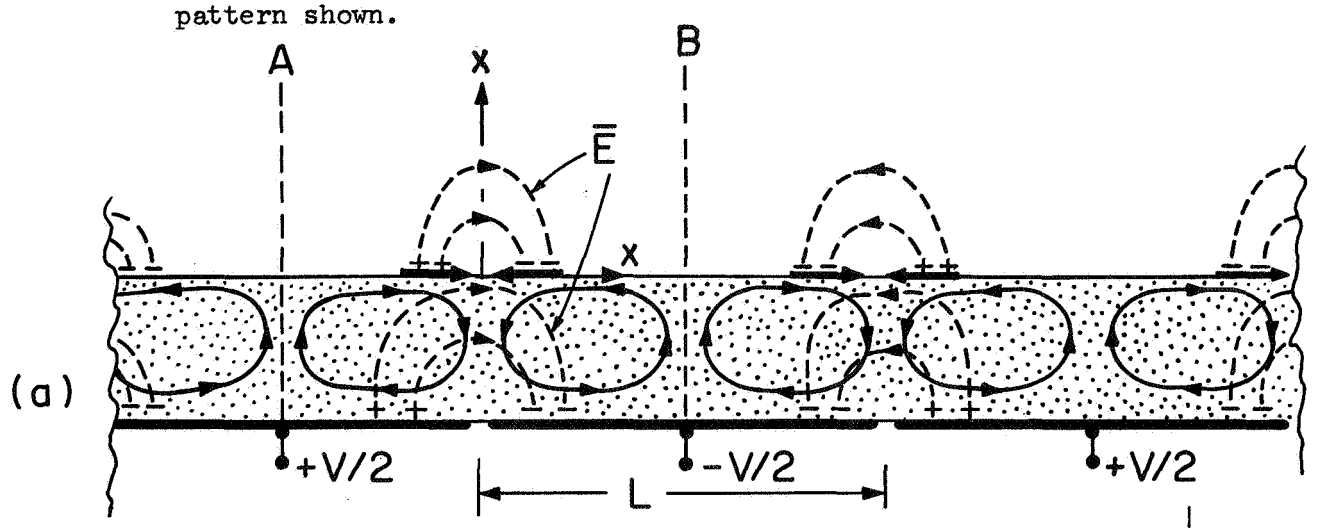

b) Cellular convection resulting from instability that tends to dominate the pumping motions of (a).

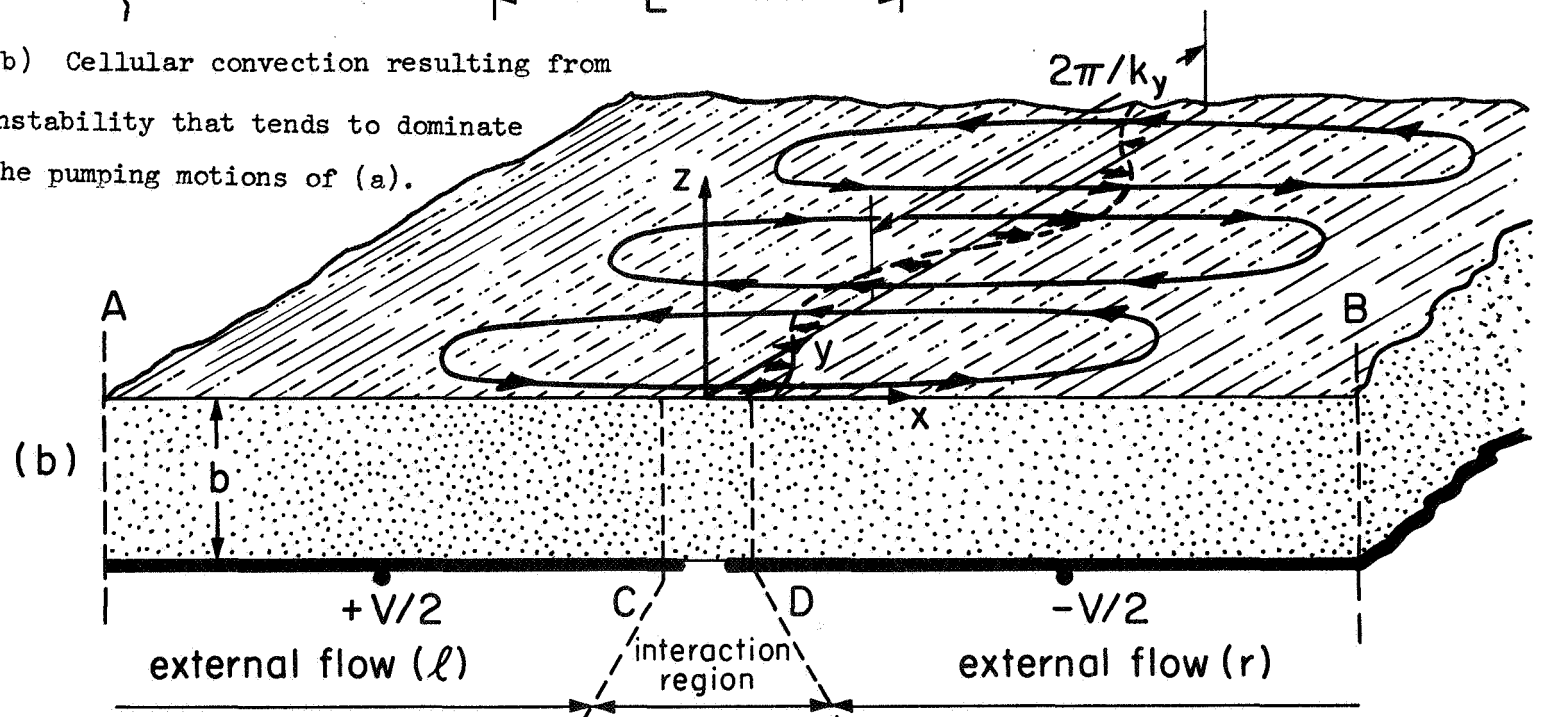

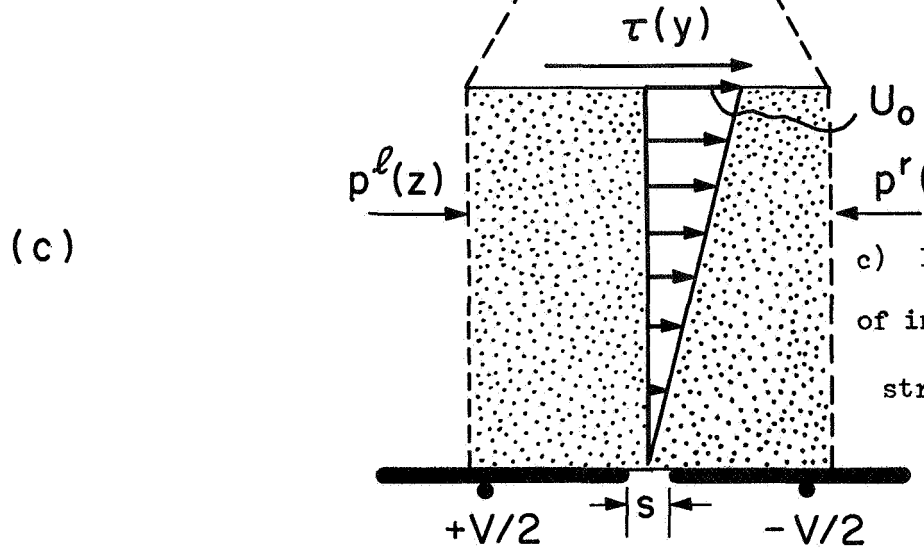

c) Interaction region where coupling of interfacial convection and shear stress gives instability.

would give rise to these motions. They are the consequence of an instability related to the manner in which the convection alters the distribution of the surface charge, and hence the distribution of surface force density. In terms of the section of fluid shown in Fig. 2c, an interfacial motion in the x direction leads to a redistribution of surface charge, hence a surface force density that tends to encourage further the surface motion. This is true whether the motion is to the right or left.

A layer of liquid in the region C-D of Fig. 2b is subject to a net surface force $\tau(y)$ acting in the x direction (per unit length in the y direction), which tends to make the section "tip" to one side or the other. The resulting motion in the x direction is inhibited by the viscous stresses of the surrounding fluid which flows in a direction of least resistance: a flow pattern with the fluid leaving the interaction region C-D at one y location, and returning to that region flowing in the opposite x direction at another location along the y axis. Cells form which have that wavelength $\hat{\lambda}$ $2\pi/k_y$ in the y direction, which assures the least impedance of the motion. In a typical experiment, cellular motions in the plane of the interface (Fig. 2b) can easily dominate those in the x-z plane (Fig. 2a), even though the latter are created by a simple pumping action while the former result from instability.

II. THE MODEL

A. Outline

There are three attributes of the phenomenon that we wish to predict; the flow pattern (in particular the wavelength in the y direction), the voltage required for incipience, and the velocity of the cellular motion.

The coupling of fluid and field makes the mathematical description nonlinear. Thus, it is desirable to proceed by separating the effects of

viscous retardation from the electroconvective driving force. The fluid layer is divided into "external flow regions" A-C and D-B in Fig. 2b, and an "interaction region" C-D. In the external flow regions, the fluid is visualized as being essentially free of surface shears and set in motion by a pressure rise across the interaction region. Then, the electrical shear stress is averaged over the x dimension of the layer and visualized as concentrated in the interaction region. Finally, the regions are "married up" by requiring that the velocities and pressure rise be self-consistent in a steady flow condition. These three steps in the analysis are outlined in the following sections.

The separation of the layer into the three regions is in part a conceptual convenience. Once the model has been formulated, it should be evident that what we are actually doing is separating the stabilizing and destabilizing effects, which need be only roughly identified with the regions of the fluid layer. In reality, the "interaction" and "external" flow regions overlap. The distinction is made here only as a convenient way of separating the viscous and electrohydrodynamic effects.

B. External Flow

In many cases of interest, the fluids are rather viscous, with induced velocities relatively small. Thus, a high Reynolds number is not likely, and creep flow approximations are justified. Ignoring inertial effects and taking advantage of the fact that there is no steady-state charge in the bulk, the Navier-Stokes equation becomes

$$\nabla p = \mu \nabla^2 \overline{v} \qquad (4)$$

where p and $\overline{v}$ are the fluid pressure and velocity, and the effects of the mass density, ρ, are ignored.

The gravitational force does not contribute to the dynamics and is ignored. In addition, conservation of mass is written

$$\nabla \cdot \bar{v} = 0 \tag{5}$$

For convenience, the velocity is constrained to be in the x-y plane. Since the surface in the external regions is free of shear stress, the derivative of $\bar{v}$ with respect to z must vanish at z = 0. Assuming no slip at the bottom, $\bar{v}$ must vanish at z = -b. It is consistent with these conditions to expand the fluid velocity and pressure as a Fourier series in the z direction while assuming a periodic dependence of wavelength $2\pi/k_y$ in the y direction.

$$\bar{v} = \sum_{\substack{n=1 \\ (odd)}}^{\infty} \{U_n(x)\cos k_y y \bar{i}_x + V_n(x)\sin k_y y \bar{i}_y\} \cos \frac{n\pi z}{2b} \tag{6}$$

$$p = \sum_{\substack{n=1 \\ (odd)}}^{\infty} P_n(x) \cos k_y y \cos \frac{n\pi z}{2b} \tag{7}$$

It follows from the components of Eq. (4) and Eq. (5) that the Fourier amplitudes must satisfy the ordinary differential equations

$$DP_n = \mu[D^2 - \beta_n^2]U_n \tag{8}$$

$$-k_y P_n = \mu[D^2 - \beta_n^2]V_n \tag{9}$$

$$DU_n + k_y V_n = 0 \tag{10}$$

where

$$\beta_n^2 = (n\pi/2b)^2 + k_y^2 \tag{11}$$

Equations (8) - (10) combine to give

$$[D^2 - \beta_n^2][D^2 - k_y^2]U_n = 0 \tag{12}$$

$$P_n = \mu[D^2 - \beta_n^2]DU_n/k_y^2 \tag{13}$$

$$V_n = - D\, U_n/k_y \tag{14}$$

In the following it is assumed that β_n and k_y are positive. This is convenient because the regions to the right and left in Fig. 2b are taken as unbounded in the + and -x directions respectively (L>> b). Appropriate solutions to Eqs. (12) and (13) to the right (r) and left (ℓ) are then

$$U_n^{(r)}_{\ell} = A_n^{(r)}_{\ell} \exp(\mp k_y x) + B_n^{(r)}_{\ell} \exp(\mp \beta_n x) \tag{15}$$

$$P_n^{(r)}_{\ell} = \pm \frac{\mu}{k_y}\left(\frac{n\pi}{2b}\right)^2 A_n^{(r)}_{\ell} \exp(\mp k_y x) \tag{16}$$

These solutions are to be spliced together at x = 0 where it is required that the velocity be in the x direction. From Eqs. (14) and (15)

$$B_n^{(r)}_{\ell} = -k_y A_n^{(r)}_{\ell}/\beta_n \tag{17}$$

Moreover, from conservation of mass, $U_n^r\ (x = 0) = U_n^{\ell}\ (x = 0)$, or from Eqs. (15) and (17),

$$A_n^r = A_n^{\ell} \tag{18}$$

Thus, from Eqs. (16)

$$P_n^r - P_n^{\ell} = 2\frac{A_n^r \mu}{k_y}\left(\frac{n\pi}{2b}\right)^2 \tag{19}$$

and it follows that the pressure jump at the origin is expressed as

$$(p^r - p^{\ell})\Big|_{x=0} = \sum_{\substack{n=1 \\ (\text{odd})}}^{\infty} \frac{2A_n^r \mu}{k_y}\left(\frac{n\pi}{2b}\right)^2 \cos k_y y \cos\frac{n\pi z}{2b} \tag{20}$$

This jump in pressure in the neighborhood of the origin (x = 0) is due to the shear stress at the interface. The stress in turn depends on the fluid velocity at the interface, which is designated as $U_o \cos k_y y$ with U_o at present undetermined. Viscous shear stress transmits the effect of the electrical surface shear stress into the bulk of the fluid, where the velocity profile varies from a maximum at the interface to zero at z = -b. In the simple model developed here, the velocity profile at x = 0 will be taken as linear in z;

$$v_x(0,y,z) = U_o\left(1 + \frac{z}{b}\right) \cos k_y y \tag{21}$$

It follows from Eqs. (6), (15) and (17) that

$$A_m^r = \frac{8U_o}{(m\pi)^2} \Big/ \left[1 - \frac{k_y}{\beta_m}\right] \tag{22}$$

Thus, from Eqs. (20) and (22), the total force per unit length (in the y direction) on the interaction region due to the external flow is

$$\int_{-b}^{0} (p^r - p^\ell)\Big|_{x=0} dz = 8\mu\, U_o F \cos k_y y \tag{23}$$

where

$$F = \sum_{\substack{m=1 \\ (\text{odd})}}^{\infty} \sin\left(\frac{m\pi}{2}\right) \Big/ \left[(k_y b)(m\pi)(1 - k_y/\beta_m)\right]$$

For a given pressure jump, Eq. (23) shows that the velocity is maximum for that wavelength in the y direction which minimizes F. The dependence of F on bk_y is shown in Fig. 3. Because the interaction region is modeled with the periodicity in the y direction included only quasi-one-dimensionally, the function F reflects the total dependence of the flow on the transverse wavelength, $2\pi/k_y$. Thus the wavenumber of the impending instability can be immediately predicted.

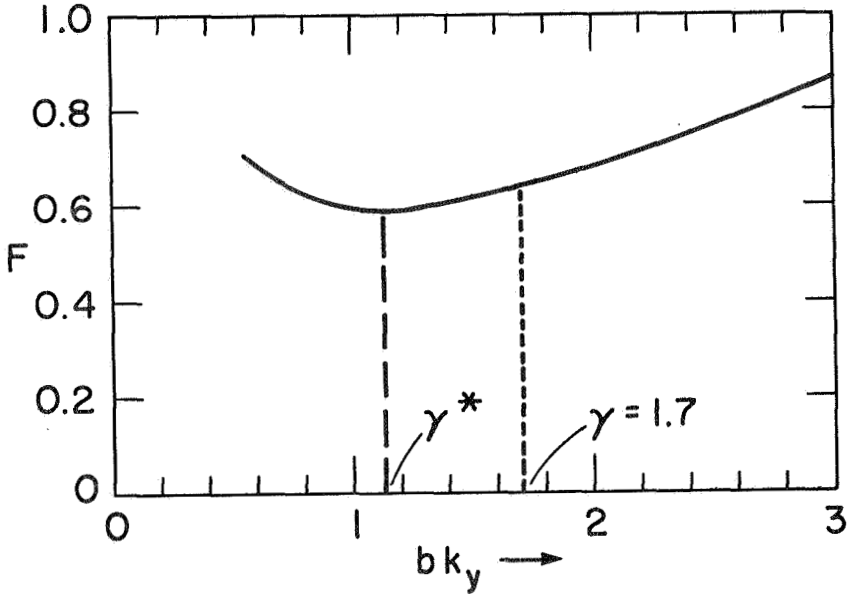

Fig. 3 Dependence of summation defined by Eq. (23) on bk_y.

$$k_y = 1.15/b \tag{24}$$

At this critical wavenumber, F = 0.592.

C. Electrohydrodynamic Coupling

In the interaction region, the velocity is in the x direction. For now, the interfacial velocity is considered independent of y, but nevertheless will later be expressed as a function of y having the same harmonic dependence on that coordinate as the other variables. The basic simplification of the electrohydrodynamics resulting from separating the flow into the three regions comes from the representation of the velocity as being uniform over the interaction region. The potential distribution imposed by the electrodes is to be expanded over the basic period 2L. However, interest will be confined to cases where $b \ll L$.

The potential throughout the fluid and region above is expanded in series of the form

$$\phi = \sum_{p=-\infty}^{+\infty} \Phi_p(z) e^{-j\frac{p\pi x}{L}} \tag{25}$$

where $\overline{E} = -\nabla\phi$.

The appropriate solutions to Laplace's equation having this form are

$$\Phi_p^a = C_p e^{-|\alpha_p| z} \tag{26}$$

$$\Phi_p^b = F_p \sinh \alpha_p z + C_p \cosh \alpha_p z \tag{27}$$

where (a) and (b) denote the regions above and below the interface respectively, and $\alpha_p = p\pi/L$. The constants in these last two equations have been chosen to make the potential continuous at the interface. The first of two conditions on F_p and C_p is that the potential at $z = -b$ is V/2 for $-L < x < 0$ and -V/2 for $0 < x < L$. In terms of the Fourier series

$$\phi_b(z=-b,x) = \sum_{p=-\infty}^{\infty} -\frac{V}{2jp\pi}(\cos p\pi - 1)\exp(-jp\pi x/L) \tag{28}$$

The second condition is that charge be conserved at the interface.

$$U_o \frac{\partial}{\partial x}\left(\varepsilon_o \frac{\partial \phi_a}{\partial z} - \varepsilon \frac{\partial \phi_b}{\partial z}\right) - \sigma \frac{\partial \phi_b}{\partial z} = 0 \tag{29}$$

It follows that C_p and F_p are given by

$$C_p = \frac{-(jU_o\alpha_p \varepsilon - \sigma)F_p}{jU_o|\alpha_p|\varepsilon_o} = \frac{V(\cos \pi p - 1)(\sigma - jU_o\alpha_p\varepsilon)}{2\pi pj[\cosh \alpha_p b(jU_o\alpha_p\varepsilon - \sigma) + \sinh \alpha_p b(jU_o|\alpha_p|\varepsilon_o)]} \tag{30}$$

The net surface force per unit length in the y direction is the integral of the surface charge density multiplied by E_x,

$$\tau = \int_{-L}^{L} \left(\varepsilon_o \frac{\partial \phi_a}{\partial z} - \varepsilon \frac{\partial \phi_b}{\partial z}\right)\Big|_{z=0} \left(\frac{\partial \phi_a}{\partial x}\right)\Big|_{z=0} dx$$

$$= 2L \sum_{p=-\infty}^{+\infty} -j\varepsilon\alpha_p^2 F_p C_p^* \tag{31}$$

where C_p^* is the complex conjugate of C_p. Using Eq. (30), Eq. (31) becomes

$$\tau = \frac{16\,\varepsilon LV^2 \varepsilon_o U_o \sigma}{(2\pi)^2} \sum_{\substack{p=1 \\ (\text{odd})}}^{\infty} \alpha_p^3/p^2[(\sigma \cosh\alpha_p b)^2 + U_o^2\alpha_p^2(\varepsilon \cosh \alpha_p b + \varepsilon_o \sinh \alpha_p b)^2] \tag{32}$$

It is at this point in the derivation that the harmonic dependence on y is taken into account in a quasi-one-dimensional manner. It is assumed that

the dependence of τ on y, brought about because the surface velocity is in fact a function of y, is slow enough that it can be accounted for by Eq. (32) evaluated with $U_o \to U_o \cos k_y y$. Even more, because it is the square of the velocity that appears in the denominator of Eq. (32), U_o is retained in the denominator without substituting a y dependence. With these approximations, Eq. (32) can be written as

$$\tau = \frac{16\,\varepsilon\varepsilon_o}{(2\pi)^2\sigma}\left(\frac{V}{b}\right)^2 U_o \cos k_y y\, G\left(\frac{b}{L}, \frac{\varepsilon_o}{\varepsilon}, R_e\right) \tag{33}$$

where

$$G = \sum_{p=1}^{\infty} \frac{L}{bp^2}(b\alpha_p)^3/(\cosh \alpha_p b)^2\left\{1 + \frac{(b\alpha_p)^2}{2} R_e^2\left[1 + \frac{\varepsilon_o}{\varepsilon}\tanh(b\alpha_p)\right]^2\right\}$$

and $R_e = \varepsilon U_o/\sigma b$. The dependence of G on b/L with $R_e = 0$ is shown in Fig. 4. Note that in the limit $R_e = 0$, G does not depend on $\varepsilon/\varepsilon_o$ and in particular, as $b/L \to 0$, $G \to 1.08$.

D. Self-Consistent Flow

The force per unit length given by Eq. (33) is now used to account for the pressure jump at the origin, as depicted in Fig. 2c, with the coupling between field and fluid represented in an average way by

$$\int_{-b}^{o} (p^r - p^\ell)\Big|_{x=0} dz = \tau \tag{35}$$

Note that, because the pressure jump is evaluated at x = 0, the viscous losses within the interaction region are lumped with those from the external flows.

Equation (23) is now used to express the left-hand side of Eq. (35) and τ is given by Eq. (33). The resulting expression requires that the pressure jump generated by the interfacial motion be balanced by the pressure drop due to viscous stresses in the external flow.

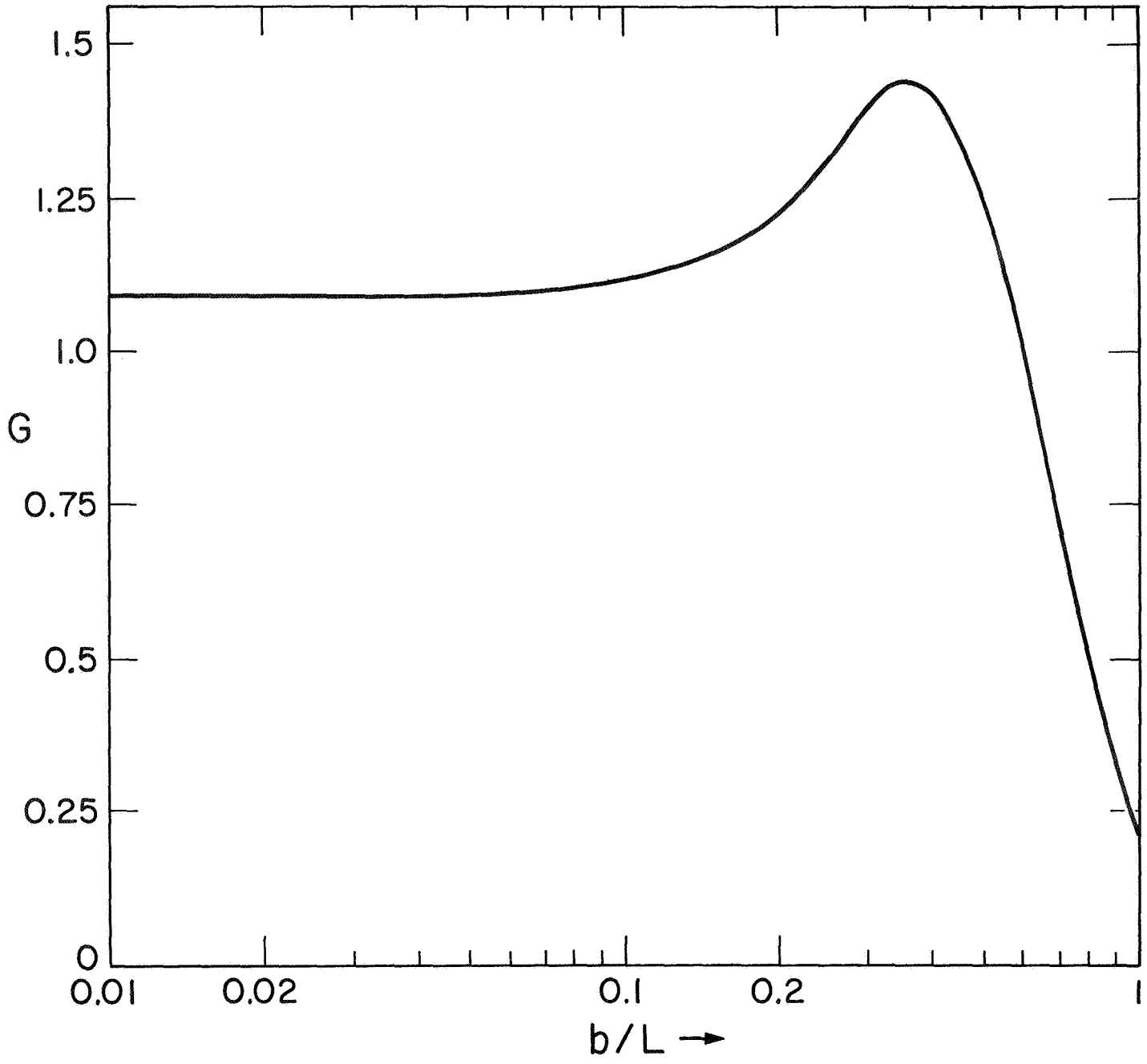

Fig. 4 Dependence of G on b/L with $R_e = 0$. The definition of G is given by Eq. (33).

$$8\mu\, U_o F \cos k_y y = \frac{16\,\varepsilon\varepsilon_o}{(2\pi)^2\sigma}\left(\frac{V}{b}\right)^2 G U_o \cos k_y y \qquad (36)$$

For a self-consistent flow, $U_o \cos k_y y$ can be canceled from this expression and Eq. (36) then takes the normalized form

$$H_e = \sqrt{2\pi^2\, F/G} \qquad (37)$$

where the electric Hartmann number $H_e = (V/b)\sqrt{\varepsilon\varepsilon_o/\mu\sigma}$. Remember that F is a function of the wavelength $2\pi/k_y$ (Fig. 3). In an experiment, the voltage is raised (H_e increased) until there is a value of k_y such that Eq. (37) is satisfied. Thus, condition (37) is first satisfied where F has its least value of 0.592 and the wavenumber k_y is as given by Eq. (24).

Instability is incipient with $R_e = 0$, and hence the condition for incipience follows from Eq. (37) as

$$H_e = 3.42/G^{\frac{1}{2}}\left(\frac{b}{L}\,,\ \frac{\varepsilon}{\varepsilon_o}\,,\ 0\right) \qquad (38)$$

with G given by Fig. 4. For example, in the limit $b/L \to 0$, the critical condition is $H_e = 3.28$.

The surface velocity is included in the denominator of Eq. (32), i.e., the dependence of G on R_e, so that Eq. (37) can also be used to approximate the steady cell velocity established once H_e exceeds the value given by Eq. (38). The normalized peak surface velocity is R_e which, given the normalized applied voltage H_e, can be found from Eq. (37). This dependence of R_e on H_e is summarized in Fig. 5. As the electric Hartmann number H_e is raised, instability is incipient at the value given by this plot with $R_e = 0$. A further increase in H_e results in a steady rate of convection given in normalized form by R_e. Thus, the electric Reynolds number R_e determines the rate at which the convection takes place, while the electric Hartmann number H_e determines its incipience.

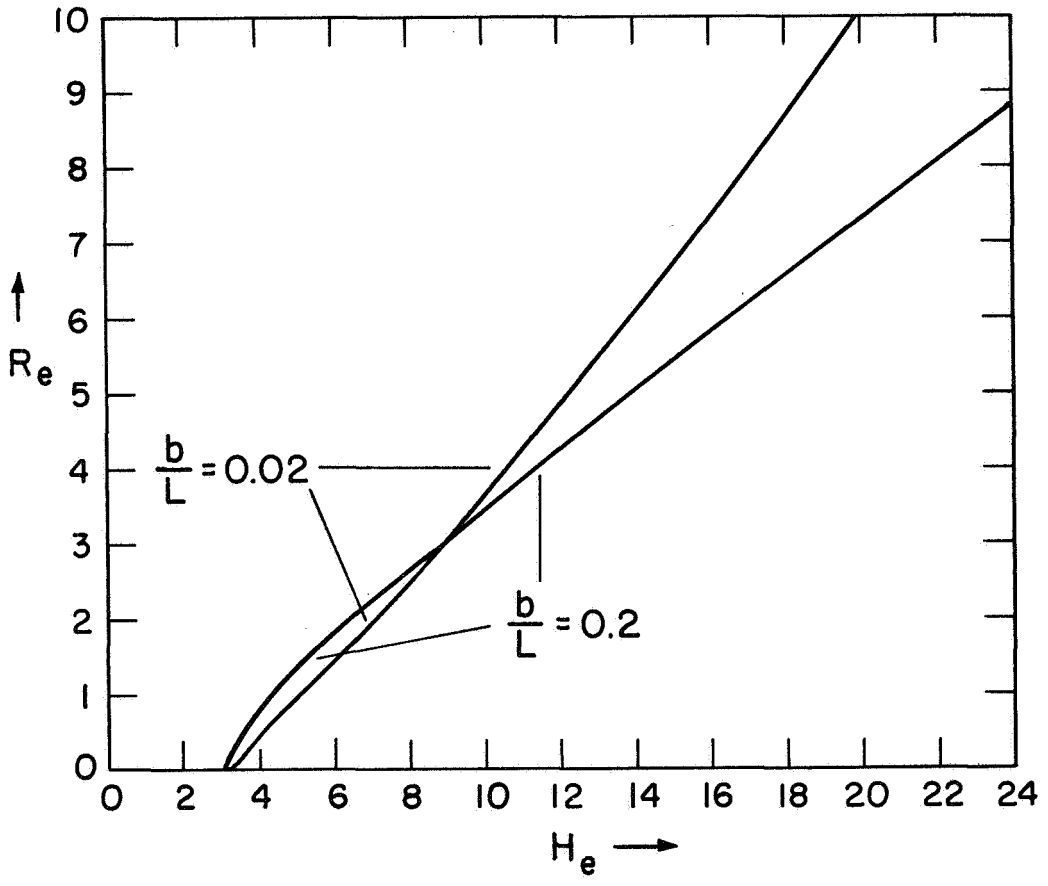

Fig. 5 The electric Reynolds number R_e is the normalized peak cell velocity, while the electric Hartmann number H_e is the normalized applied voltage. Thus, there is a threshold in voltage at which the convection sets in, and the plot shows how the cell velocity then increases with voltage. The case b/L = 0.02 is very nearly the same as $b/L \to 0$.

III. EXPERIMENT

A. Arrangement and Observation

The form of electroconvective instability described in the previous sections is remarkably simple to demonstrate. A pair of planar metallic electrodes is placed side by side in the bottom of an insulating container with a spacing, s, of 2 mm. between the abutting edges (Figs. 2b and 2c). Then, the electrodes are leveled and covered by a layer of corn oil to a depth b that is varied between 2 and 20 mm. In the experiments described here, the container has x and y dimensions of 19 and 15 cm respectively, although these dimensions are not critical so long as the relative cell wavelengths are small.

The motion is observed by introducing small air bubbles onto the interface. Although such bubbles can have a drastic influence on the motions of highly insulating fluids, they remain a passive means of flow visualization in the corn oil.

As a potential difference between the electrodes is increased, a threshold is reached at which cellular convection occurs in the plane of the interface. Typical cells are shown in Figs. 6a and 6b, where time exposure of the bubble motions result in a record of the streamlines. The two photographs include the same area of interface, hence illustrate the increase in cell wavelength that accompanies increasing the depth.

The streamlines predicted by the theoretical model are shown in Fig. 6c, scaled for comparison to Fig. 6b. Viewed from the side, the bulk motion is observed to be in the x-y plane, justifying Eq. (6).

B. Wavelength and Voltage for Onset of Instability

The wavelength of the incipient instability, $\lambda = 2\pi/k_y$, is twice the distance between the cell centers shown in Fig. 6. Thus, it is a straightforward matter to take the data of Fig. 7 from photographs. The solid curve

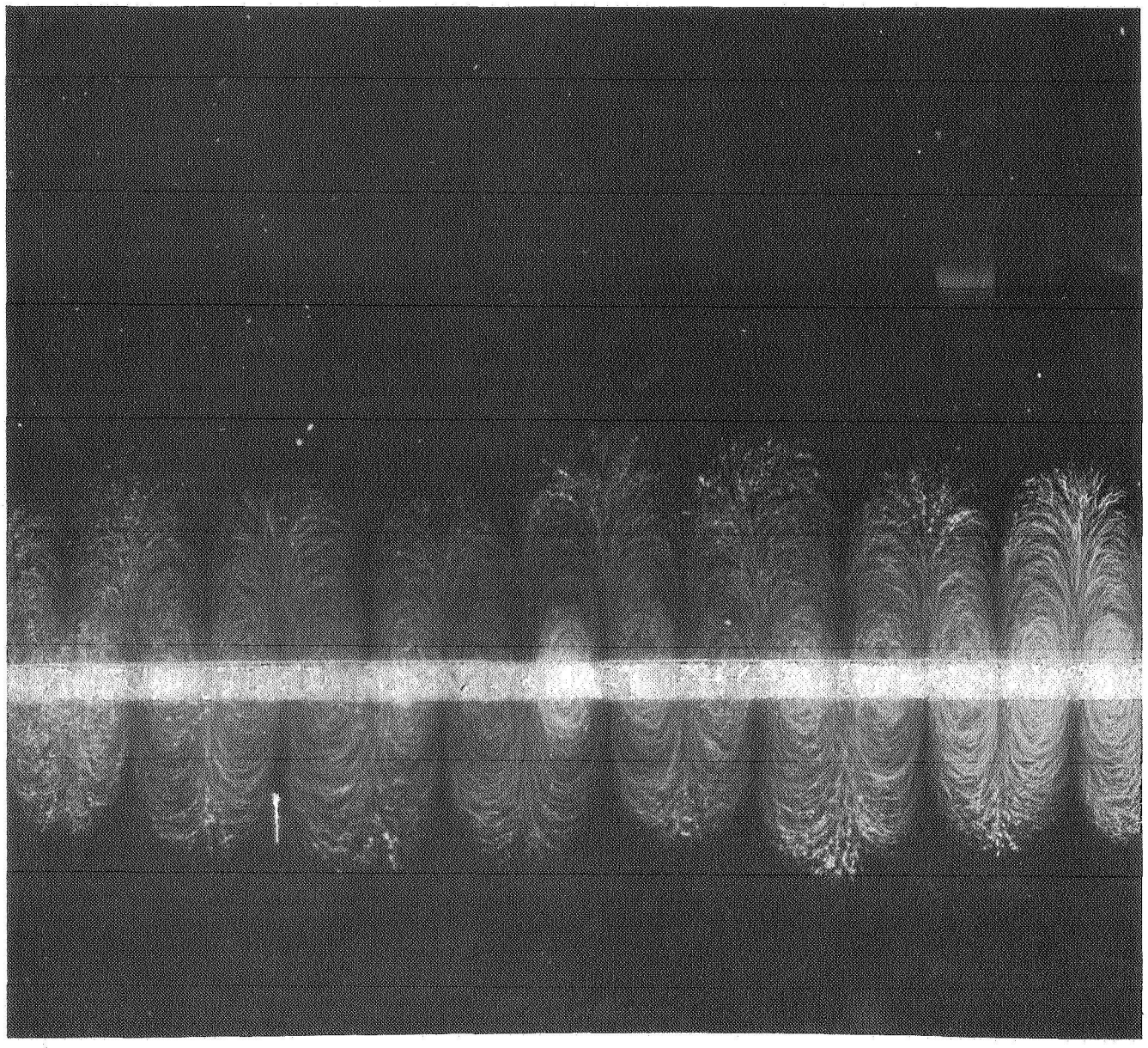

Fig. 6 Cellular convection resulting from electroconvective instability, as seen looking down at the interface (looking in the -z direction in Fig. 2b). a & b) Time exposure photographs in which streamlines are made visible by entraining small bubbles on the liquid interface. Depths b are 3mm and 7 mm respectively, and voltages are 3.35 and 4.8 kv. Note lengthening of wavelength with depth, as predicted by Eq. (24). Photographs are to the same scale in both cases. Streaks in (b) are modulated by a forced vibration of the apparatus to give a measure of the fluid velocity; longer wavelengths indicate higher velocity.

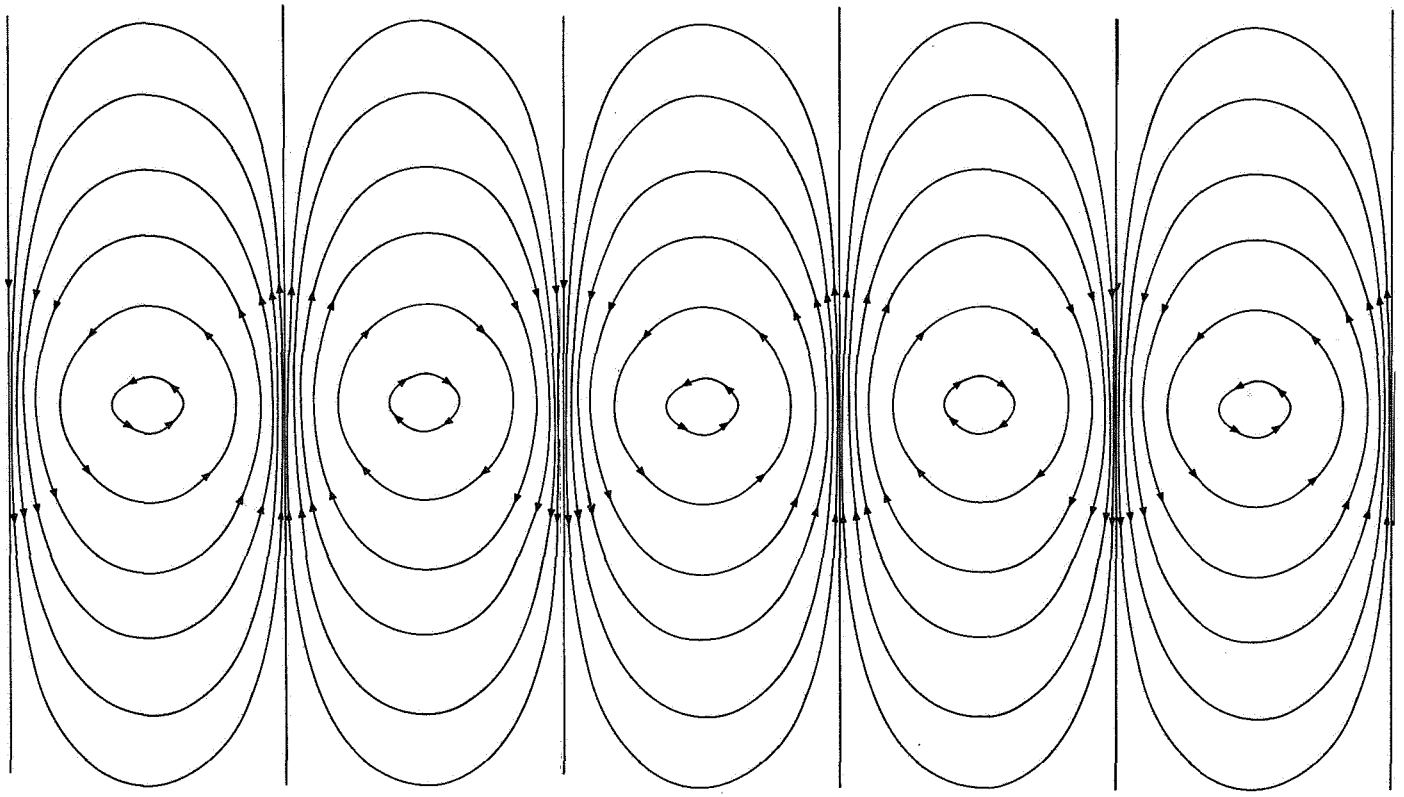

c) Streamlines at interface corresponding to predictions of Eqs. (6), (15) (17), and (22) for (b), with $bk_y = \gamma^*$.

of Fig. 7 is predicted by Eq. (24), while the dashed curve would be predicted by Eq. (24) if $1.15 \rightarrow 1.7$ ($\gamma^* \rightarrow \gamma$ in Fig. 3). This difference between the theoretical and observed wavelengths is not unreasonable if it is recognized that the mode selection involves the minimization of a slowly varying function (Fig. 3). There is only a 10% difference between the values of F corresponding to the two curves of Fig. 7.

The measured voltage for onset of cellular convection is presented in Fig. 8, together with the prediction of Eq. (38) in the limit $b/L \rightarrow 0$. Here the agreement between prediction and experiment is better than would be expected, in view of approximations inherent to the model.

C. Cell Velocity

Streak photographs, taken for the fully developed cells, provide the measurements of peak cell velocity U_o as a function of voltage, V, shown in Fig. 9. Use of the physical parameters of Fig. 8, together with b = 0.7 cm, gives the direct correspondence between U_o and R_e, and between V and H_e summarized by the alternative ordinates and abscissas of the figure. The solid curve is predicted by Eq. (37) in the limit $b/L \rightarrow 0$ (see Fig. 5).

Here again, the agreement between the approximate model and the observations is closer than might be expected. The ordinary Reynolds number $U_o b\rho/\mu$ is about 5 as U_o reaches 4 cm/sec. Thus, the discrepancy between prediction and observation for velocities greater than 5 cm/sec. is probably due to inertial effects, which are ignored in the model.

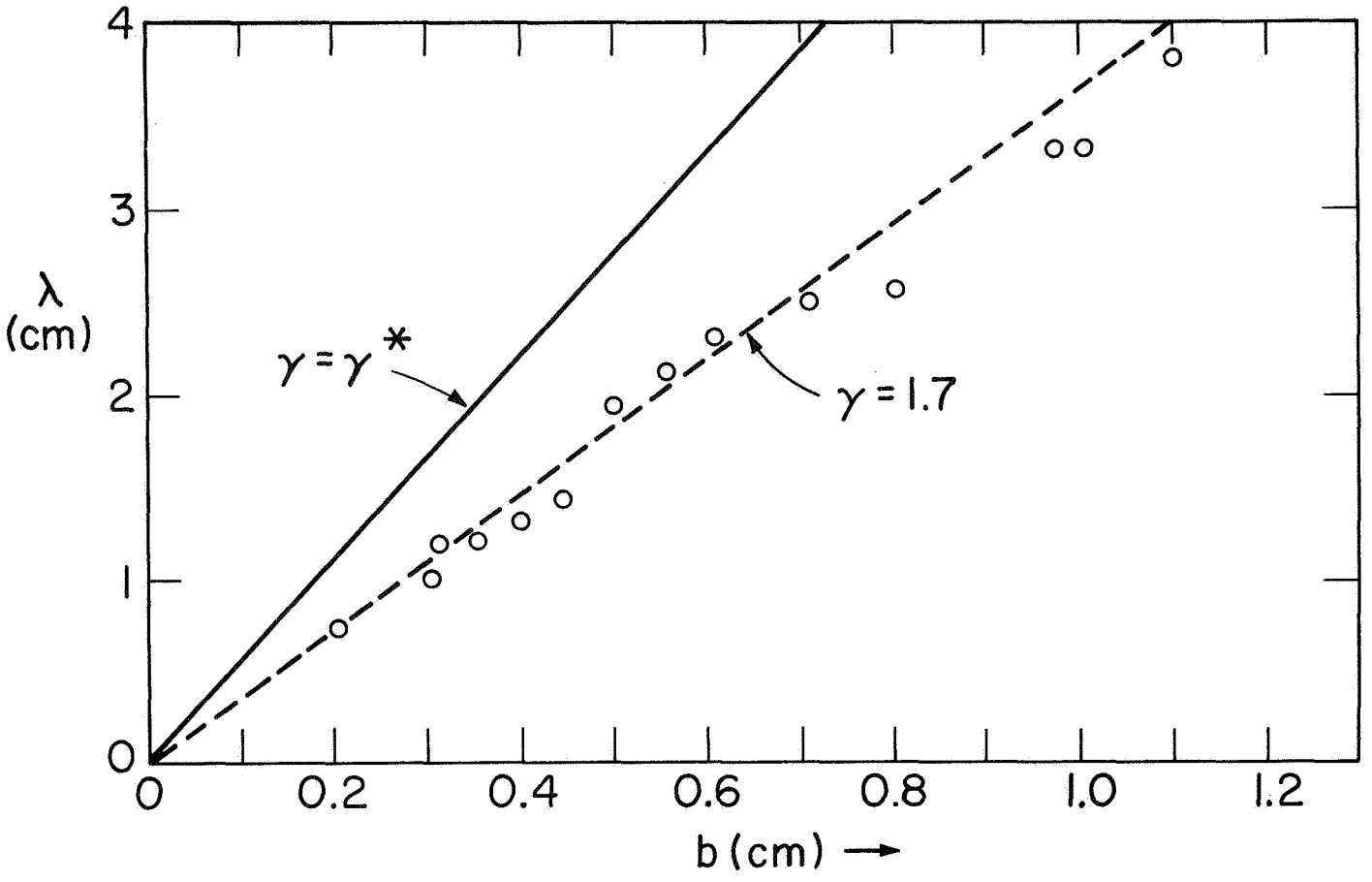

Fig. 7 Wavelength $\lambda = 2\pi/k_y$ of incipient instability as a function of the liquid depth, b. The solid curve is predicted by Eq. (24) while the points represent experimental observations. The dotted line illustrates the prediction that would be obtained by using a value of γ corresponding to a value of F only 7% greater than the minimum value (see Fig. 3).

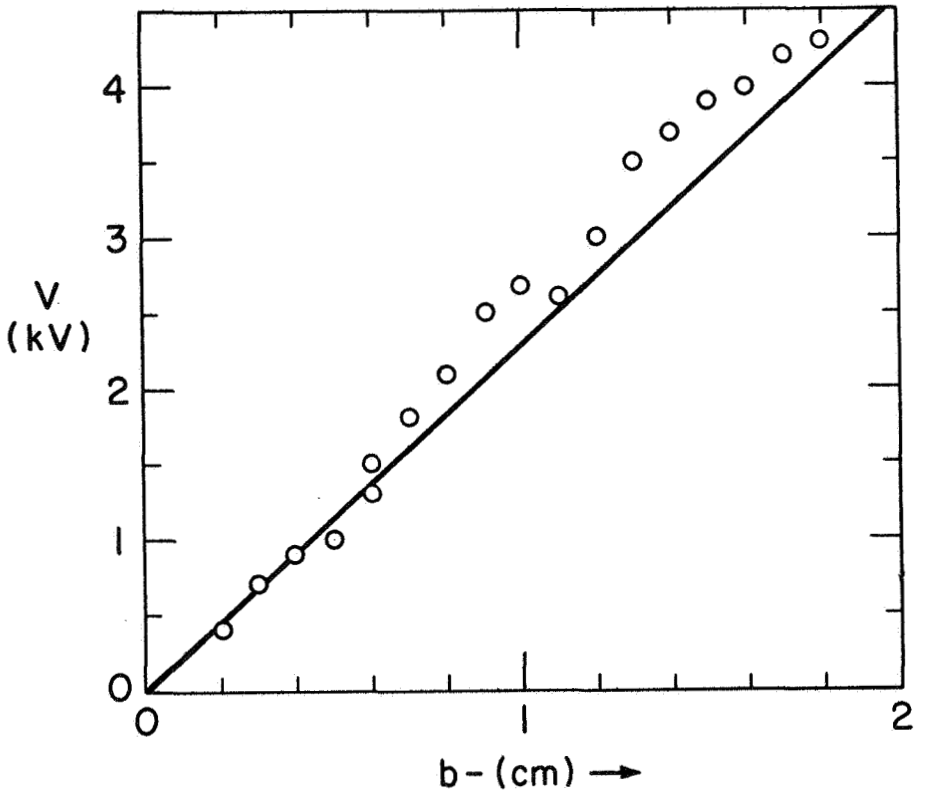

Fig. 8 Voltage for onset of instability as a function of fluid depth. The solid line is predicted by $H_e = 3.28$. In the experiment, corn oil is used with $\mu = 5.46 \times 10^{-2}$ kg(ms)$^{-1}$, $\sigma = 2.2 \times 10^{-11}$(ohm-m)$^{-1}$ $\varepsilon = 3.1\ \varepsilon_o$.

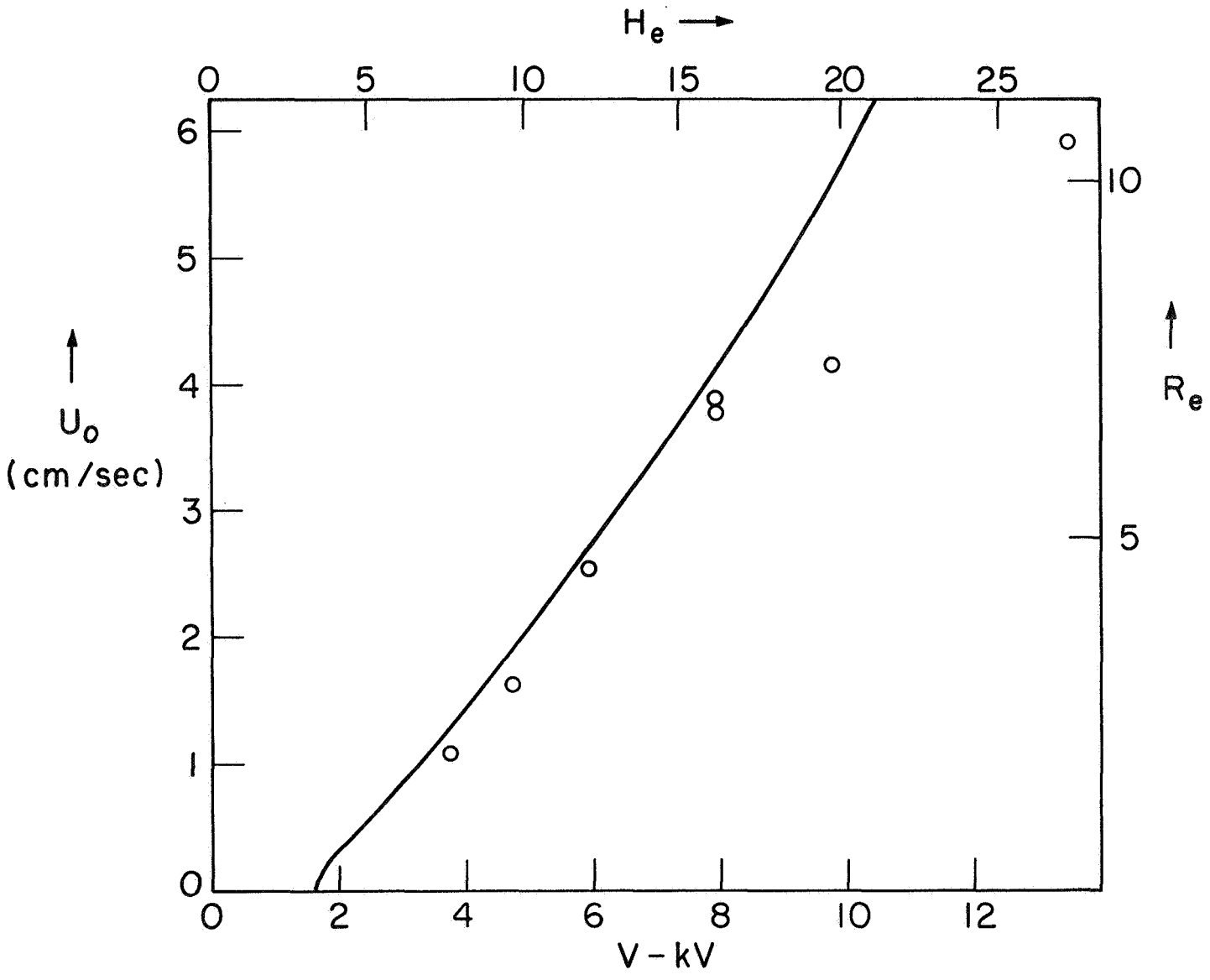

Fig. 9 Peak cell velocity U_o as a function of the applied voltage. The depth b = 7 mm and fluid parameters are as given in Fig. 8. The theoretical curve shown follows from the results of Fig. 5 with $b/L \to 0$, and the relations $U_o = \sigma b R_e/\varepsilon$, $V = H_e b\sqrt{\mu\sigma/\varepsilon\varepsilon_o}$. With $U_o = 4$ cm/sec., the ordinary Reynolds number based on the depth is about 5.

IV. CONCLUDING REMARKS

This case study gives quantitative insight to a class of instabilities characterized by incipience at a critical electric Hartmann number (Eq. 3) and ensuing steady convection at a rate proportional to an electric Reynolds number (Eq. 2). The case recommends itself as the basis for understanding related phenomena, because it can be easily reproduced in the laboratory, and meaningfully represented by a relatively simple model.

There are three types of electrohydrodynamic interactions that appear related to the case described. The most obvious of these occurs in a diversity of situations in which liquid-liquid or liquid-gas interfaces are stressed by an electric field (Taylor 1966, Smith & Melcher 1967). The pumping motion resulting from shear stresses at the interface may be dominated by a form of instability analogous to that discussed here. A recent review has focused attention on this type of interaction (Melcher & Taylor 1969) to provide an overview of physical situations in which surface shear pumping and electroconvective instability have been investigated. Included in this review is an alternative model (Jolly 1968) for the instability described here; a model more appropriate for the experiments in which b is comparable to L.

Certain bulk instabilities found as a uniform ion current is passed through a highly insulating initially static layer of liquid also appear to have this electroconvective nature, with a critical electric Hartmann number for incipience (Schneider & Watson 1969). The convection resulting from this class of instabilities may be related to electrooptical liquid crystal effects currently being investigated for image-processing purposes (Heilmeier, et al 1968), and is certainly related to high-field conduction processes through insulating liquids (Watson & Schneider 1967)(Lewis & Secker 1967).

A third type of instability occurs in conjunction with an equilibrium flow; in pumps with ions flowing in the direction of equilibrium convection (Stuetzer 1959) or in channels with a transverse ion current (Jorgensen 1968). Although the velocity profile and other particulars brought in by the equilibrium convection and characterized by the ordinary Reynolds number are certainly involved (Lin 1955), many electrohydrodynamic bulk flow instabilities appear to have an electroconvective nature also.

Acknowledgments:

E. Paul Warren assisted in experiments. This work was supported by NASA Grant NGL 22-009-014.

REFERENCES

HEILMEIER, G. H., ZANONI, L.A., & BARTON, L.A., 1968 Proc. of the Institute of Electrical and Electronic Engineers, 56, No. 7, 1162-1171.

JOLLY, D.C., 1968 M.S. Thesis, Dept. of Electrical Engineering, Massachusetts Institute of Technology, Cambridge, Mass.

JORGENSEN, J. E., 1968 Ph.D. Thesis, Dept. of Electrical Engineering, Massachusetts Institute of Technology, Cambridge, Mass.

LEWIS, T.M. & SECKER, P.E. 1968, Publication 1578, National Academy of Sciences Washington, D. C., 87-95.

LIN, C. C. 1955, The Theory of Hydrodynamic Stability, Cambridge University Press, 1-139.

MALKUS, W.V.R, & VERONIS, G., 1961, Phys. Fluids, 4, No. 1, 13.

MELCHER, J.R., & TAYLOR, G. I. 1969 Electrohydrodynamics: A Review of the Role of Interfacial Shear Stresses, Annual Review of Fluid Mechanics, Vol. I.

SCHNEIDER, J. M. & WATSON, P.K. 1969, "Electroconvective Stability of Space-Charge-Limited Currents in Dielectric Liquids", paper presented at Symposium on Electrohydrodynamics, sponsored by International Unions of Applied Mechanics and Pure and Applied Physics, Massachusetts Institute of Technology, March 31-April 1,2, 1969.

SMITH, C. V., & MELCHER, J. R. 1967, Phys. Fluids, 10, No. 11, 2315-2322.

STUETZER, O.M., 1959 Phys. Fluids 2, No. 6, 642-648.

TAYLOR, G. I., 1966, Proc. Roy. Soc., (London) A291, 159

TURNBULL, R. J. & MELCHER, J. R., "Electrohydrodynamic Rayleigh-Taylor Bulk Instability", to be published, Phys. Fluids.

WATSON, P. K. & SCHNEIDER, J. M., "Transient Space-Charge-Limited Conduction in Liquid Dielectrics", Annual Report of Conference on Electrical Insulation and Dielectric Phenomena, Pub. 1578, National Academy of Sciences, Washington, D. C., pp. 95-99.